Article

Class IA PI3Ks regulate subcellular and functional dynamics of IDO1

Alberta Iacono[1], Andrea Pompa[2,3], Francesca De Marchis[3], Eleonora Panfili[1], Francesco A Greco[4], Alice Coletti[4], Ciriana Orabona[1], Claudia Volpi[1], Maria L Belladonna[1], Giada Mondanelli[1], Elisa Albini[1,4], Carmine Vacca[1], Marco Gargaro[1], Francesca Fallarino[1], Roberta Bianchi[1], Carine De Marcos Lousa[5,6], Emilia MC Mazza[7] [iD], Silvio Bicciato[8] [iD], Elisa Proietti[1], Francesca Milano[9], Maria P Martelli[9], Ioana M Iamandii[1], Mariona Graupera Garcia-Mila[10] [iD], Judith Llena Sopena[10] [iD], Phillip Hawkins[11], Sabine Suire[11] [iD], Klaus Okkenhaug[12] [iD], Anne-Katrien Stark[12], Fabio Grassi[13], Michele Bellucci[3], Paolo Puccetti[1], Laura Santambrogio[14] [iD], Antonio Macchiarulo[4] [iD], Ursula Grohmann[1,15,*,†] [iD] & Maria T Pallotta[1,†]

Abstract

Knowledge of a protein's spatial dynamics at the subcellular level is key to understanding its function(s), interactions, and associated intracellular events. Indoleamine 2,3-dioxygenase 1 (IDO1) is a cytosolic enzyme that controls immune responses via tryptophan metabolism, mainly through its enzymic activity. When phosphorylated, however, IDO1 acts as a signaling molecule in plasmacytoid dendritic cells (pDCs), thus activating genomic effects, ultimately leading to long-lasting immunosuppression. Whether the two activities—namely, the catalytic and signaling functions—are spatially segregated has been unclear. We found that, under conditions favoring signaling rather than catabolic events, IDO1 shifts from the cytosol to early endosomes. The event requires interaction with class IA phosphoinositide 3-kinases (PI3Ks), which become activated, resulting in full expression of the immunoregulatory phenotype *in vivo* in pDCs as resulting from IDO1-dependent signaling events. Thus, IDO1's spatial dynamics meet the needs for short-acting as well as durable mechanisms of immune suppression, both under acute and chronic inflammatory conditions. These data expand the theoretical basis for an IDO1-centered therapy in inflammation and autoimmunity.

Introduction

Indoleamine 2,3-dioxygenase 1 (IDO1) is a cytosolic enzyme that contributes to immune suppression and tolerance in a variety of settings (Grohmann *et al*, 2003b; Puccetti & Grohmann, 2007; Grohmann & Bronte, 2010). IDO1 effects are mainly mediated by dendritic cells (DCs), and they involve deprivation of tryptophan and the production of immunomodulatory kynurenines. As a result, IDO1-expressing DCs mediate multiple effects on T lymphocytes, including inhibition of proliferation, apoptosis, and

1 Department of Experimental Medicine, University of Perugia, Perugia, Italy
2 Department of Biomolecular Sciences, University Carlo Bo, Urbino, Italy
3 Institute of Biosciences and Bioresources, National Research Council of Italy, Perugia, Italy
4 Department of Pharmaceutical Sciences, University of Perugia, Perugia, Italy
5 Centre for Biomedical Sciences, School of Clinical and Applied Sciences, Leeds Beckett University, Leeds, UK
6 Center for Plant Sciences, Faculty of Biological Sciences, University of Leeds, Leeds, UK
7 Istituto Clinico Humanitas, Rozzano, Italy
8 Department of Life Sciences, University of Modena and Reggio Emilia, Modena, Italy
9 Department of Medicine, University of Perugia, Perugia, Italy
10 Bellvitge Biomedical Research Institute (IDIBELL), Hospitalet de Llobregat, Spain
11 Babraham Institute, Cambridge, UK
12 Department of Pathology, University of Cambridge, Cambridge, UK
13 Institute for Research in Biomedicine, Bellinzona, Switzerland
14 Englander Institute for Precision Medicine, Weill Cornell Medicine, New York, NY, USA
15 Department of Pathology, Albert Einstein College of Medicine, Bronx, NY, USA
*Corresponding author. Tel: +39 075 585 8240; E-mail: ursula.grohmann@unipg.it
†These authors contributed equally to this work as senior authors

differentiation toward a regulatory phenotype (Fallarino *et al*, 2002; Fallarino *et al*, 2003; Fallarino *et al*, 2006; Puccetti & Grohmann, 2007).

IDO1-mediated effects also include non-enzymic functions, namely, intracellular signaling events that, initiated by phosphorylation of specific domains (i.e., immunoreceptor tyrosine-based inhibitory motifs; ITIMs) in the enzyme, are involved in reprogramming gene expression and in inducing a stable regulatory phenotype in both plasmacytoid (pDCs) and conventional DCs (cDCs), as purified from mouse spleens (Mondanelli *et al*, 2017b; Grohmann *et al*, 2017). IDO1's ITIM phosphorylation is triggered by the cytokine transforming growth factor (TGF-β) in DCs (Pallotta *et al*, 2011; Bessede *et al*, 2014; Pallotta *et al*, 2014; Mondanelli *et al*, 2017a; Mondanelli *et al*, 2019a). In specific settings, the activation of metabotropic glutamate receptor 4 (Volpi *et al*, 2016) is likewise involved in the overall immunomodulatory action of IDO1.

The IDO1 signaling pathway requires a tyrosine kinase of the Src family, specifically, Fyn in pDCs (Pallotta *et al*, 2011) and Src in cDCs (Bessede *et al*, 2014; Volpi *et al*, 2016; Mondanelli *et al*, 2017a). The tyrosine kinase phosphorylates IDO1's ITIMs, thus creating docking sites for the Src homology region 2 domain-containing phosphatase-1 (SHP-1) and SHP-2. Moreover, the use of the LY294002 inhibitor indicated that IDO1 signaling also involves the catalytic activity of phosphoinositide 3-kinases (PI3Ks) (Pallotta *et al*, 2011; Volpi *et al*, 2016), although the functional role of those enzymes and their action (i.e., whether upstream or downstream of IDO1's ITIMs phosphorylation) has been unclear.

PI3Ks constitute a family of lipid kinases coordinating several intracellular signaling pathways in the modulation of growth, metabolism, and immunity (Koyasu, 2003; Engelman *et al*, 2006; Thorpe *et al*, 2015). Among their multiple roles, members of the PI3K family also affect intracellular trafficking of vesicles and proteins (Vanhaesebroeck *et al*, 2010). Class IA PI3Ks, the best characterized isoforms, consist of a catalytic subunit (p110α, p110β, or p110δ) in complex with one of five distinct regulatory subunits, collectively referred to as "p85s". In contrast, the p110γ subunit belongs in the class IB family, and it does not efficiently bind p85s (Vanhaesebroeck *et al*, 2010). Following receptor activation, class IA PI3Ks are recruited to the plasma membrane, where p85 inhibition of p110 is relieved, and p110 phosphorylates its substrate. Alternatively, p85 can bind a phosphorylated tyrosine within a YxxM (where "x" indicates any amino acid) motif of another protein, and this event leads to a conformational change in p85 that translates into the activation of the pre-associated p110 subunit (Geering *et al*, 2007; Thorpe *et al*, 2015). However, the nonselective properties of LY294002 did not allow us to identify the specific PI3K subunits involved in IDO1 signaling.

In the present study, we investigated the role of specific PI3K subunits in the noncatalytic activity of IDO1 in cell lines expressing different IDO1 constructs and in pDCs freshly purified from mouse spleens. We found that, in addition to ITIMs, IDO1 contains a YENM motif that is responsible for direct binding of p85 and consequent activation of class IA PI3K p110 subunits, which events lead to IDO1 anchoring to early endosomes (EE) and activation of the immunoregulatory IDO1 pathway in pDCs.

Results

Activation of class IA PI3K p110 subunits is required for IDO1 signaling and immunosuppressive effects in pDCs

To investigate the role of specific PI3K subunits in the IDO1 signaling pathway, we first performed a meta-analysis of public microarray data to evaluate the expression of genes coding for PI3K subunits (i.e., both regulatory and catalytic) in pDCs purified from mouse lymphoid and non-lymphoid organs. A dominance was found in the expression of class IA p110 (mainly *Pik3cd*, coding for p110δ) and p85 (mainly *Pik3r1*, coding for p85α) subunits (Fig 1A). Interestingly, whereas p110α and p110β are ubiquitously expressed, p110δ expression is generally restricted to cells of the immune system (Okkenhaug & Vanhaesebroeck, 2003). Moreover, p110δ activity has been shown to foster anti-inflammatory effects in macrophages and DCs (Aksoy *et al*, 2012).

We thus investigated the effects of selective class IA PI3K p110 inhibitors (Fig 1B and Materials and Methods) in the catalytic versus signaling functions of IDO1. We used A66, TGX-221, and CAL-101 inhibitors, targeting p110α, β, and γ/δ, respectively. The LY294002 nonselective inhibitor was used as a positive control (Pallotta *et al*, 2011; Volpi *et al*, 2016). Whereas IDO1 enzymatic activity is normally revealed by production of L-kynurenine (Kyn; the main IDO1 product), the downstream effects of IDO1 signaling involve induction of *Ido1* and *Tgfb1* expressions, an effect that initiates a positive immunoregulatory feedback loop in pDCs lasting over time (Pallotta *et al*, 2011; Bessede *et al*, 2014; Pallotta *et al*, 2014; Albini *et al*, 2018). We quantified Kyn production (Fig 1C) and expression of *Ido1* as well as *Tgfb1* transcripts (Fig 1D) in pDCs incubated with IFN-γ—the main inducer of IDO1 catalytic activity (Grohmann *et al*, 2003b)—or with TGF-β—which triggers the IDO1's signaling pathway (Pallotta *et al*, 2011; Pallotta *et al*, 2014; Mondanelli *et al*, 2017a; Mondanelli *et al*, 2019b)—in the presence or absence of PI3K inhibitors. As expected, IFN-γ significantly increased Kyn production by pDCs. However, no inhibitor significantly impaired IDO1's catalytic activity, regardless of the presence of a cytokine (Fig 1C). In contrast, A66, CAL-101, and TGX-221—albeit to a lesser extent than A66 and CAL-101—significantly opposed the increased expression of *Ido1* and *Tgfb1* transcripts by TGF-β (Fig 1D), suggesting a critical role for all class IA p110 isoforms in the IDO1 signaling pathway (Pallotta *et al*, 2011).

To better clarify the role of class IA PI3K p110 subunits in the immunosuppressive potential of pDCs conditioned with TGF-β, we used the skin test assay, an established protocol for measuring the *in vivo* induction of antigen-specific immunoreactivity—as opposed to tolerance—in DCs (Puccetti *et al*, 1994; Grohmann *et al*, 2002; Grohmann *et al*, 2007; Pallotta *et al*, 2011; Mondanelli *et al*, 2017a). We sensitized mice with the HY peptide (containing the *H-2D*b epitope of male minor transplantation antigen) presented by CD8− DCs—constituting an immunostimulatory, splenic cDC subset (Grohmann *et al*, 2003a)—administered in combination with a minority fraction of pDCs (5%), after treatment with A66, TGX-221 or CAL-101 for 1 h prior to conditioning with TGF-β. The LY294002 nonselective inhibitor was used as a positive control (Pallotta *et al*, 2011; Volpi *et al*, 2016). At 2 weeks of mouse priming, we assessed immune reactivity by intrafootpad challenge with the HY peptide in the absence of DCs, as described (Puccetti *et al*, 1994; Grohmann
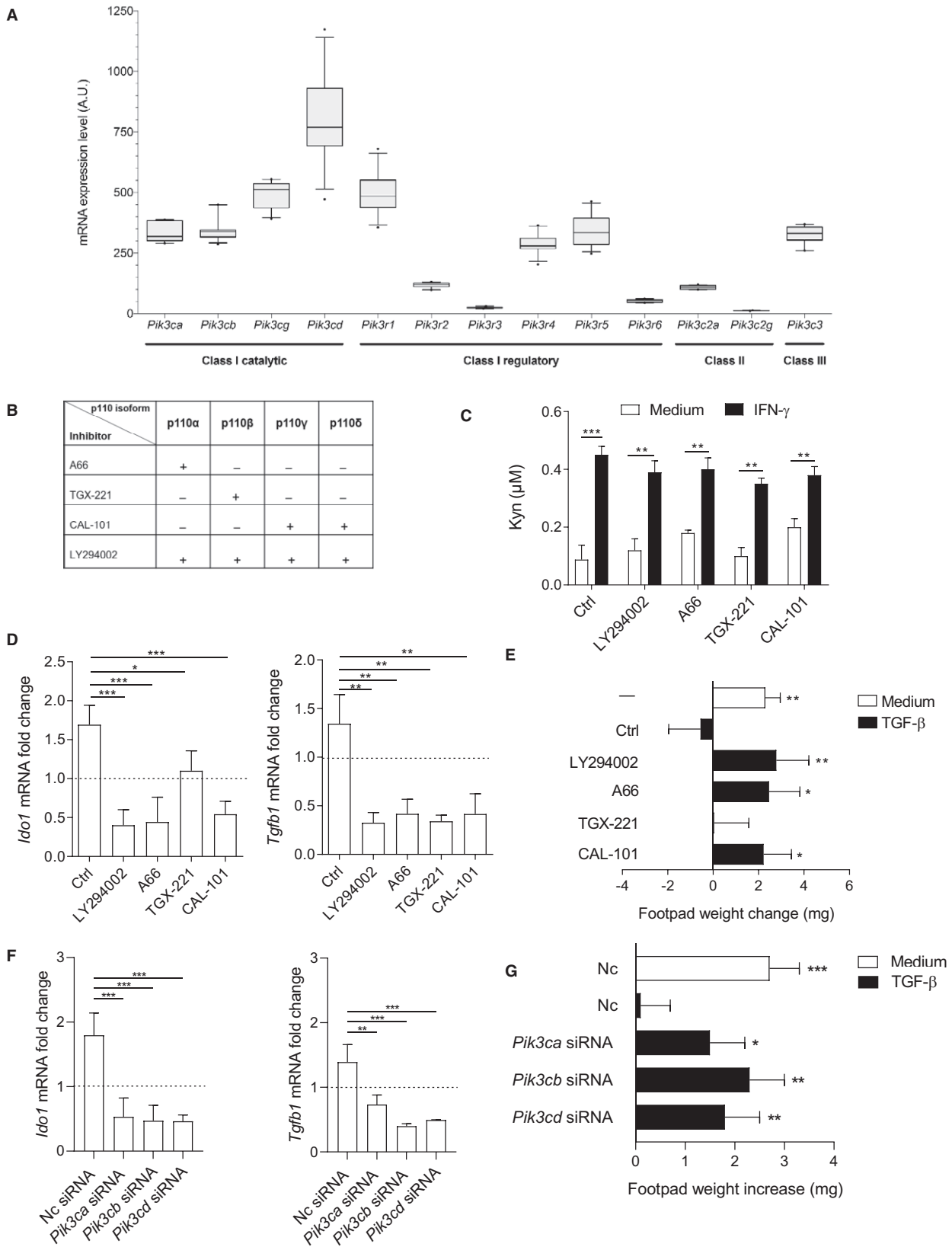
Figure 1.

◀

Figure 1. Class I PI3K p110 activity is required for IDO1 signaling and immunosuppressive effects in pDCs.

A   Expression of transcripts coding for PI3K subunit genes in pDCs ($n = 12$ biological replicates). In the box plot, the middle, the bottom, and the top of the box represent the median, the 1st quantile, and the 3rd quantile, respectively; the height of the box is given by the difference between the 3rd and the 1st quantiles (IQR, interquartile range); the whiskers length is 1.5 times the interquartile range. Data points beyond the whiskers represent values more extreme than 1.5 times the interquartile range above or below the 3rd or the 1st quantile, respectively.

B   Selectivity of PI3K inhibitors used in this study.

C   Kyn levels in culture supernatants of pDCs incubated for 24 h with medium alone (Ctrl) or IFN-γ after 1 h pretreatment with PI3K inhibitors.

D   Real-time PCR analysis of *Ido1* and *Tgfb1* transcripts in pDCs stimulated for 18 h with TGF-β, in the presence or absence (Ctrl, control) of catalytic PI3K inhibitors, normalized to the expression of *Gapdh* and presented relative to results in untreated cells (dotted line, 1-fold).

E   *In vivo* suppression of the activity of HY-pulsed CD8⁻ DCs in combination with a minority fraction (5%) of pDCs conditioned *in vitro* with TGF-β (or medium) for 24 h in the presence or absence (Ctrl) of catalytic inhibitors as in (C). Analysis of skin reactivity of recipient mice to the eliciting peptide at 15 days is presented as change in footpad weight (experimental versus control footpads).

F   Real-time PCR analysis of *Ido1* and *Tgfb1* transcripts in pDCs transfected with p110α-, β-, δ-specific, or negative control (nc) siRNA and stimulated for 18 h with TGF-β, normalized to the expression of *Gapdh* and presented relative to results in unstimulated cells (dotted line, 1-fold).

G   *In vivo* suppression of the activity of HY-pulsed CD8⁻ DCs in combination with a minority fraction (5%) of pDCs transfected with siRNA as in (F) and conditioned *in vitro* with TGF-β (or medium) for 24 h. Analysis of skin reactivity of recipient mice to the eliciting peptide at 15 days is presented as change in footpad weight (experimental versus control footpads).

Data information: In (C-G), one representative experiment of three is shown. Data represent the mean ± SD ($n = 3$ technical replicates). Statistical analysis was performed using two-tailed unpaired Student's *t*-test (C) or ANOVA followed by post-hoc Bonferroni's test (D and F) or paired Student's *t*-test (E and G). *$P < 0.05$; **$P < 0.01$; ***$P < 0.001$.

et al, 2002; Grohmann *et al*, 2007; Pallotta *et al*, 2011; Mondanelli *et al*, 2017a). As expected, the default priming ability of immunostimulatory CD8⁻ DCs was not affected by the presence of untreated pDCs. Yet, sensitization via TGF-β−treated pDCs caused suppression of HY-specific reactivity (Pallotta *et al*, 2011), an effect not detectable in mice sensitized with pDCs preincubated with LY294002, CAL-101, or A66 but not with TGX-221 (Fig 1E).

Because the use of PI3K catalytic inhibitors may not be sufficient to accurately define the role of individual p110 isoforms in the signaling function of IDO1, we used alternative approaches to complement our data in pDCs, namely, gene-specific siRNA as well as isoform knockouts and kinase-dead isoform knock-ins for the specific PI3K p110 subunits. Wild-type pDCs were transfected with siRNA specific for p110α, β, δ, or negative control siRNA (Fig EV1A). All reagents significantly inhibited the upregulation of both *Ido1* and *Tgfb1* in pDCs (Fig. 1F) and abrogated the immunosuppressive effects conferred on pDCs administered *in vivo* after TGF-β conditioning (Fig. 1G). The finding that the TGX-221 inhibitor did not revert the immunosuppressive effects conferred on pDCs by TGF-β (yet, it did inhibit—though to a lesser extent than other inhibitors—*Ido1* and *Tgfb1* upregulation) could be due to an issue involving membrane permeability. In addition, we used pDCs purified from p110α$^{D933A/WT}$ (expressing a kinase-dead protein), PI3K p110δ$^{D910A/D910A}$ (expressing a catalytically inactive p110δ isoform), and p110γ^{KO} (lacking the kinase-expressing gene) (Juss *et al*, 2012) mice and their appropriate controls. Unlike controls, pDCs from either p110α or p110δ knock-in mice failed to upregulate *Ido1* and *Tgfb1* expressions in response to TGF-β (Fig EV1B). Intriguingly, similar results were obtained with pDCs purified from mice lacking the expression of p110γ, suggesting that class IB PI3Ks may also play an as yet undefined role in IDO1's signaling activity (Fig EV1B). Thus, class IA PI3Ks appear to be critically involved in IDO1 signaling but not catalytic functions in pDCs and, perhaps most importantly, in reprogramming pDCs toward an immunosuppressive phenotype.

IDO1 binds the PI3K p85 subunit via a YxxM motif

Because class IA p110 subunits normally complex with a p85 regulatory subunit, which in turn binds the tyrosine-phosphorylated YxxM motif of another protein (Geering *et al*, 2007; Thorpe *et al*, 2015), we investigated any occurrence of such a motif in IDO1. By alignment of amino acid sequences, we identified a conserved YENM sequence in IDO1—but not IDO2, the IDO1 paralogue (Ball *et al*, 2007) considered an ancient form of IDO1 that is not endowed with signaling functions (Pallotta *et al*, 2011)—across different species (Fig 2A). More specifically, the YENM sequence was found to be part of an antiparallel β-sheet/α-helix/β-sheet module localized outside the catalytic cleft of the large domain of the enzyme. A protein–protein docking study using the crystal structures of human IDO1 and of the human PI3K p85 SH2 domain revealed good geometrical complementarity of molecular shapes between the β/α/β module of IDO1 bearing the YENM motif and the phosphotyrosine binding site of the SH2 domain in p85 (Fig 2B).

To verify the binding of IDO1 to PI3K p85, we performed pull-down experiments using biotinylated peptides containing the tyrosine-phosphorylated or unphosphorylated Y$_{149}$ENM sequence of mouse IDO1 to precipitate the PI3K p85 subunit. Biotinylated peptides containing IDO1's ITIM1 and ITIM2 motifs phosphorylated in their tyrosine residues—previously shown to bind both SHP-1 and SHP-2 phosphatases (Pallotta *et al*, 2011)—in combination with SHP-1 and SHP-2 precipitation were used as controls. Lysates of P1.HTR mouse tumor cells, constitutively expressing the PI3K p85 subunit (Fig 2C), were incubated with the biotinylated peptides followed by streptavidin-agarose for immunoprecipitation. PI3K p85 greatly bound the phosphorylated form of the YENM-containing peptide but not the other peptides (Fig 2C). In contrast, SHP-1 and SHP-2 effectively precipitated with the pITIM1-containing peptide but not with the other peptides, suggesting that—at variance with the pYVKM motif of cytotoxic T lymphocyte antigen 4 that associates with SHP-2 (Lee *et al*, 1998; Chuang *et al*, 2000)—PI3K p85 but not the tyrosine phosphatases interact directly with the pYENM motif in IDO1. The fact that SHP-1 and SHP-2 did not precipitate efficiently with the pITIM2-containing peptide would corroborate our recent findings, which demonstrated that ITIM1 is mostly involved in the partnership with SHPs and IDO1 signaling (thus resulting in long-term IDO1 expression) and ITIM2 is more effective at binding suppressor of cytokine signaling 3 (SOCS3), which drives proteasomal degradation of IDO1 and thus shortens its half-life (Albini *et al*,
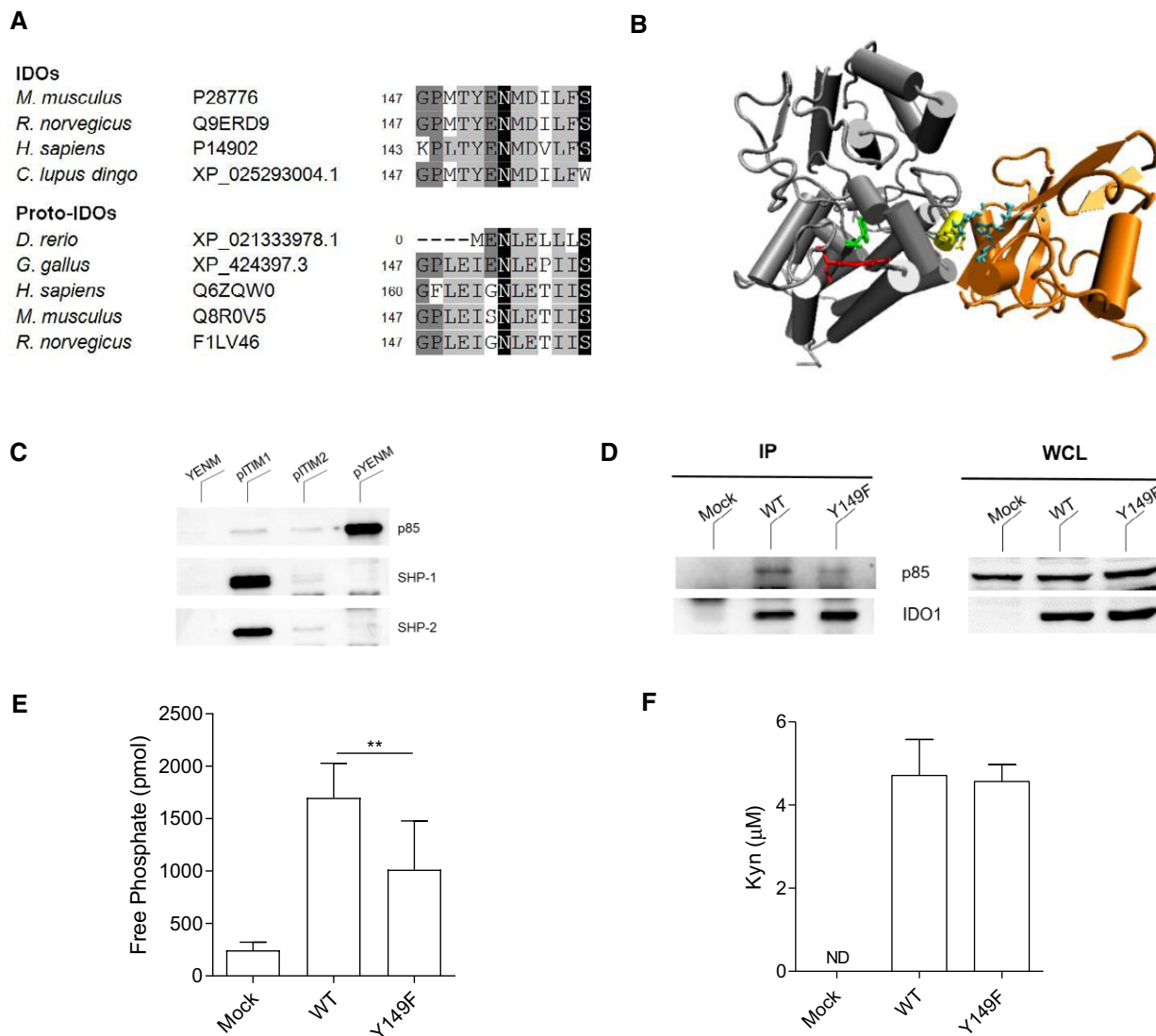
Figure 2. IDO1 contains a YENM motif that binds the PI3K p85 subunit.

A   Alignment of the amino acid sequences of IDOs restricted to the stretch of amino acids containing the YxxM motif (where x is any amino acid). Residues are highlighted based on increasing conservation level of symbols in the multiple alignments (light gray ≥ 44.4%; dark gray ≥ 66.6%; black ≥ 88.8%). IDOs, homologs of IDO1. Proto-IDOs, homologs of IDO2. Accession number for each specific gene is indicated.

B   Cartoon model of human IDO1 (gray) and the SH2 domain of PI3K p85 (orange) complex as resulting from docking study. Residues of the YENM motif are colored in yellow and shown in sticks. Residues of phosphotyrosine binding site in p85 are colored in cyan and shown in sticks. Heme and L-tryptophan are shown in sticks and colored in red and green, respectively.

C   Pull-down (PD) assay of lysates from P1.HTR cells with unphosphorylated (YENM) and tyrosine-phosphorylated IDO1 peptides (pYENM, pITIM1, and pITIM2) analyzed by sequential immunoblotting with anti-p85, anti-SHP-1, and anti-SHP-2 antibodies.

D   Immunoblotting with anti-IDO1 and anti-p85 antibodies of IDO1 immunoprecipitates obtained from P1.HTR cells transfected with IDO1.WT or IDO1.Y149F. Mock-transfected P1.HTR cells were used as a control.

E   Tyrosine phosphatase activity in anti-IDO1 immunoprecipitates from lysates of P1.HTR transfectants as in (D).

F   Kyn release over 24 h by P1.HTR transfectants as in (D).

Data information: One of two (C and D) and three (E and F) representative experiments is shown. Data represent the mean ± SD (*n* = 3 technical replicates). Statistical analysis was performed using ANOVA followed by post-hoc Bonferroni's test. **$P < 0.01$.

Source data are available online for this figure.

2017). We next performed coimmunoprecipitation experiments with an anti-mouse IDO1 antibody using lysates from P1.HTR cells (i.e., not expressing IDO1), stably transfected with the vector alone or constructs coding for mouse IDO1 wild-type (IDO1.WT) or IDO1.Y149F, a mutant lacking the phosphorylable tyrosine present in the YENM sequence (Fig EV2). The PI3K p85 subunit co-precipitated efficiently with IDO1.WT but only weakly with the IDO1.Y149F mutant (Fig 2D). The weak, yet detectable, association

of PI3K p85 with the IDO1.Y149F mutant could be due to the presence of a second YxxM motif (i.e., Y_{89}ITM) in mouse and rat but not human IDO1, which, however, appears not to be solvent exposed adequately (i.e., at the surface of the IDO1 protein) as does instead the YENM motif (see Material and Methods for data of solvent accessible surface areas, SASA) and which, therefore, may be less accessible to tyrosine phosphorylation and perhaps bound by other proteins.

To investigate the possible effects of the binding of PI3K p85 on IDO1 signaling and catalytic functions, we evaluated IDO1-associated tyrosine phosphatase activity (mediated by the SHP partners) to quantify the signaling function (Pallotta *et al*, 2011; Albini *et al*, 2017). At the same time, levels of Kyn production were measured in culture supernatants as an estimate of enzymatic activity. In P1.HTR cells transfected with IDO1.Y149F, significantly less tyrosine phosphatase activity co-precipitated as compared to cells transfected with IDO1.WT (Fig 2E). In contrast, no significant difference could be observed in terms of Kyn released by the two cell transfectants (Fig 2F). Thus, our data indicated the existence of an additional IDO1 protein partner, i.e., PI3K p85, which appears to be involved in the signaling but not catalytic activity of IDO1.

The IDO1 protein resides in both cytosol and EE in tumor transfectants

Among their multiple roles, members of the PI3K family affect intracellular trafficking of vesicles and proteins (Vanhaesebroeck *et al*, 2010). Multitasking proteins, i.e., performing more than one biologic function as does IDO1, perform multiple activities through a variety of mechanisms, including complex formation with different partners, post-translational modifications—mainly represented by phosphorylation—and also changes in subcellular location (Black, 2000). Whereas the bulk of literature data indicates a cytosolic localization of the IDO1 enzyme (Littlejohn *et al*, 2003; Honig *et al*, 2004), no information is available as to the intracellular topology of IDO1 as a signaling molecule. We therefore aimed at defining the intracellular localization of IDO1 by using a series of distinct technical approaches. By confocal microscopy of P1.HTR tumor cell transfectants stably expressing the gene construct of mouse IDO1.WT (capable of both catalytic and signaling activity), IDO1 staining revealed a diffuse localization—compatible with a cytoplasmic compartmentalization pattern—and yet discrete spots ("hotspots") were also observed, possibly indicating a locally higher expression level of the enzyme, the formation of aggregates, or the association with specific subcellular structures (Fig 3A). We next used antibodies recognizing specific markers of EE (EEA1), lysosomes (LAMP1), endoplasmic reticulum (calnexin), and Golgi apparatus (TGN-38) in combination with the anti-IDO1 antibody. The 4',6-diamidino-2-phenylindole (DAPI) reagent was used to stain nuclei. Co-staining of IDO1 and markers of subcellular organelles indicated the definite occurrence of IDO1 association with EE—but not endoplasmic reticulum (ER), Golgi apparatus, and nuclei—in addition to a diffuse IDO1 expression compatible with a cytoplasmic localization (Fig 3B). Though modest, colocalization of IDO1 with lysosomes could also be observed. To confirm the capacity of IDO1 to associate with EE, the small organelles were purified from P1.HTR cell transfectants expressing IDO1.WT, lysed, and analyzed by sequential immunoblotting with an antibody recognizing the

signaling form of IDO1—i.e., the protein as phosphorylated in its tyrosine ITIM residue (i.e., anti-pIDO1)—and the anti-IDO1 antibody. Antibodies recognizing Rab5 (i.e., a small GTPase specifically involved in the EE pathway) and Rab7 (specific for late endosomes) were also used. Mock-transfected cells were used as a control. Expression of pIDO1, IDO1, EEA1, and Rab5 but not Rab7 could be observed in EE lysates obtained from cells transfected with IDO1.WT but not from controls (Fig 3C).

By using sucrose isopycnic gradient analyses followed by Western blotting with antibodies recognizing IDO1 and markers of subcellular compartments, we next fractionated the subcellular organelles from P1.HTR cells stably transfected with mouse IDO1.WT. IDO1.WT was detectable in both low density fractions (#1–4), corresponding to cytosol, and in more dense fractions (#12–14), corresponding to subcellular organelles (Fig 3D). Stripping and reblotting with anti-EEA1, anti-LAMP1, anti-Golgin-97 (detecting the Golgi apparatus), or anti-calreticulin (detecting the endoplasmic reticulum) specific antibodies indicated that IDO1$^+$ #12 − 14 fractions paralleled the marker of EE and ER but not lysosomes and Golgi (Fig 3D). Therefore, as a whole, these data indicated that, in a tumor cell transfectant, the IDO1 protein is not just confined to cytosol but can also associate with small organelles, mainly represented by EE.

The YENM motif is required for IDO1 localization to EE

We thus investigated whether the YENM motif could be involved in IDO1 localization to EE. We evaluated the subcellular topology of the IDO1.Y149F mutant as compared to IDO1.WT. Experiments of confocal microscopy indicated that IDO1.Y149F expression associates with EEA1$^+$ organelles significantly less than IDO1.WT (Figs 4A and B). Likewise, isopycnic gradient analyses revealed that the IDO1.Y149F mutant is apparently excluded from the higher density fractions corresponding to subcellular organelles and is instead confined to the low density fractions associated with cytosol (Fig 4C and D). These data suggested that the tyrosine contained in the Y_{149}ENM motif, possibly owing to the binding of the PI3K p85 subunit, plays a major role in driving IDO1 localization to EE (Fig 3) and IDO1 signaling (Fig 2).

Activation of class IA PI3K p110 subunits is required for IDO1 EE localization and signaling in tumor transfectants

We next investigated whether a class I PI3K p110 subunit could be recruited to the PI3K p85/IDO1 complex and whether its catalytic activity would be required for IDO1 EE localization and signaling. Pull-down experiments were performed with lysates of untransfected P1.HTR cells and biotinylated peptides containing tyrosine-phosphorylated or unphosphorylated Y_{149}ENM as in Fig 2D, and Western blotting was performed with anti-PI3K p110α-, β-, γ-, or δ-specific antibodies. PI3K p110α, p110β, and even more p110δ were detected in the precipitates obtained with the pYENM-containing peptide (Fig 5A). As expected, the γ isoform could not be clearly detected in the pull-down condition with the pYENM-containing peptide (Fig. 5A). The use of PI3K p110 isoform-selective inhibitors (Fig 1B) indicated that, in P1.HTR cells transfected with IDO1.WT cells, all class IA PI3K p110 subunits are involved in IDO1 localization in EE (Fig 5B and C), whereas p110α and δ but not β are involved in the recruitment of SHP tyrosine phosphatases by IDO1
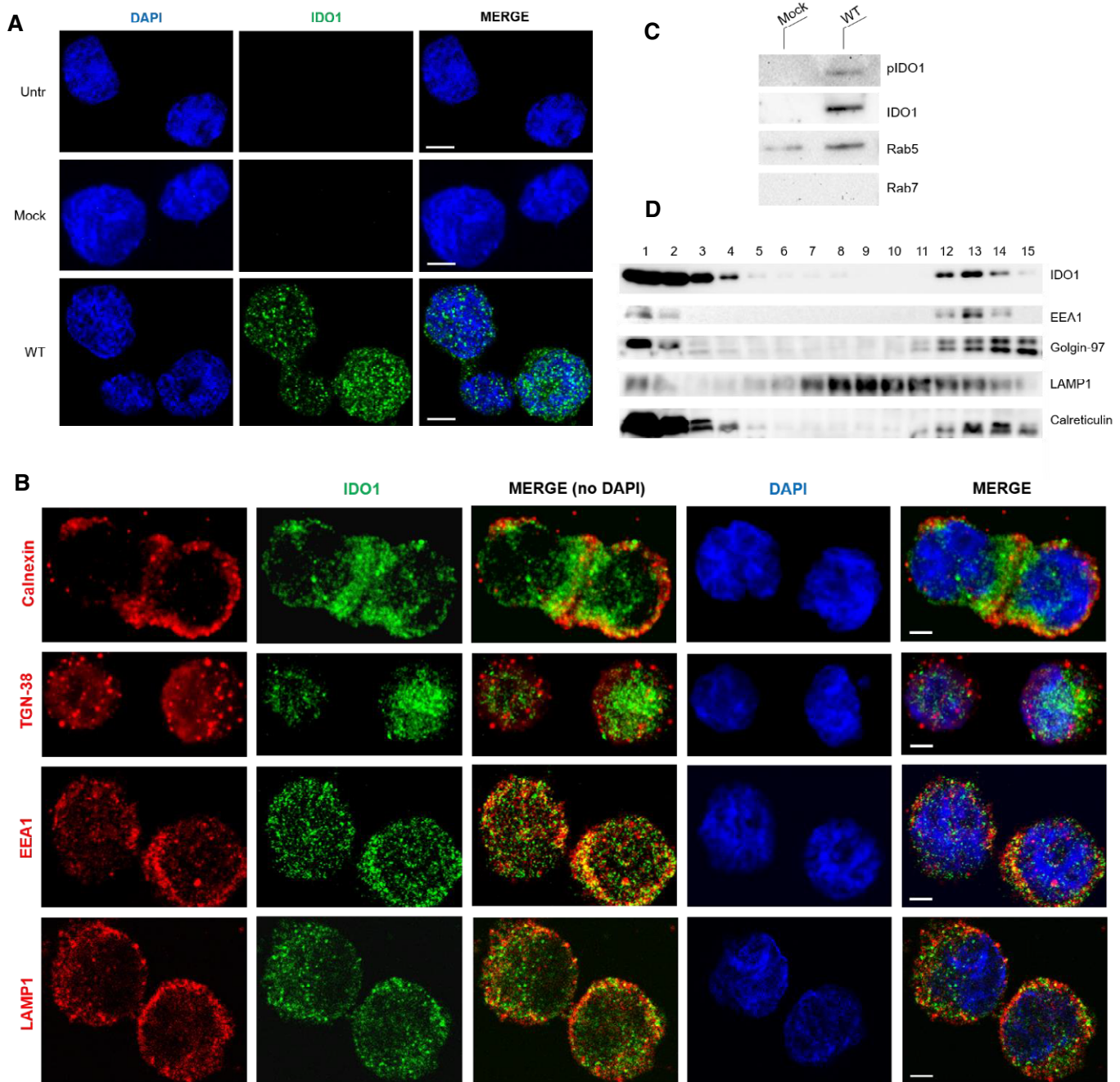
Figure 3. IDO1 colocalizes with EE in tumor transfectants.

A   Confocal immunofluorescence microscopy images of P1.HTR cells either untransfected (Untr) or transfected with IDO1.WT (WT) or vector alone (Mock) and stained with antibodies recognizing IDO1 (green). Nuclei were stained with DAPI (blue). Scale bar, 20 μm.
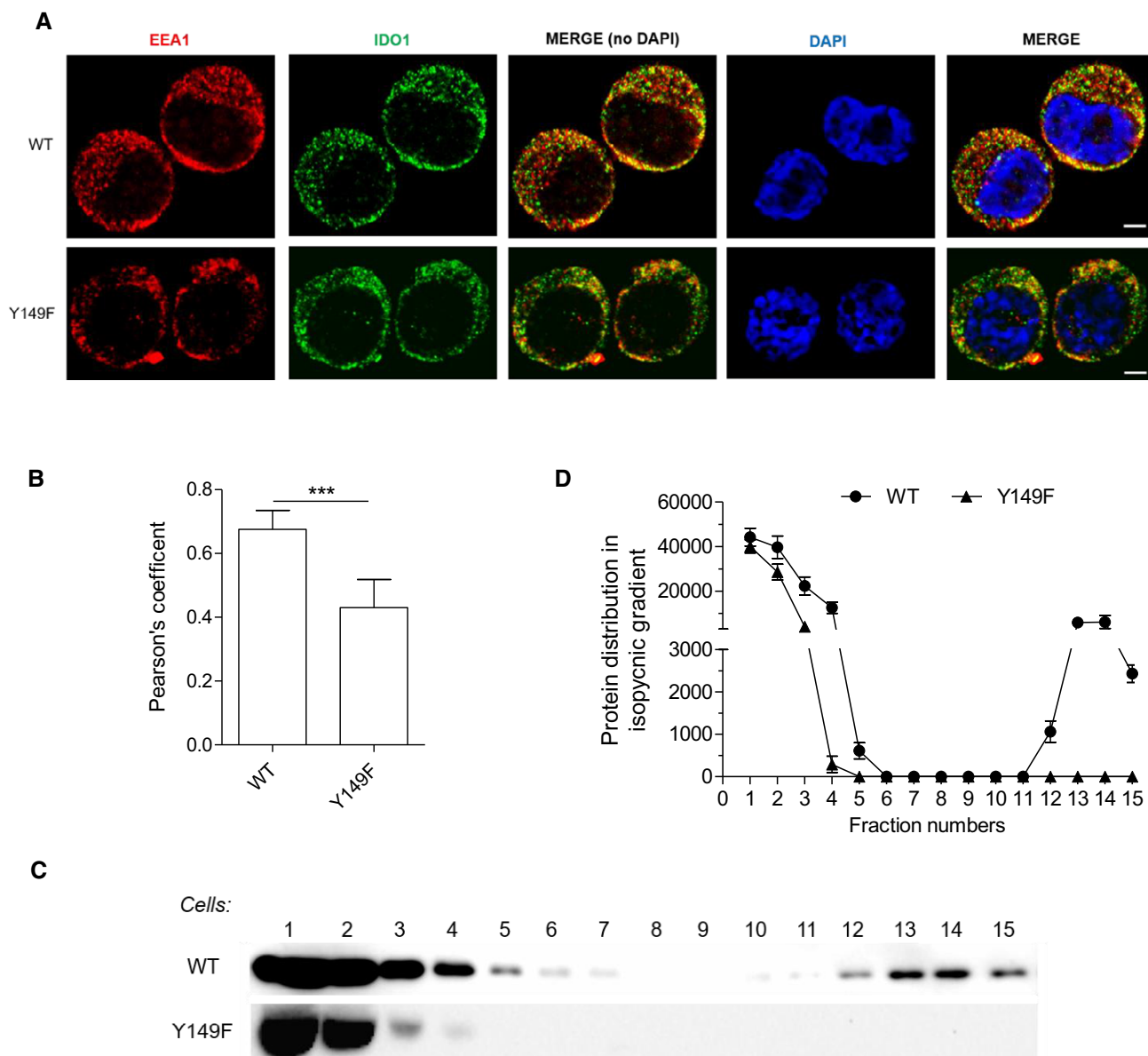
B   Confocal immunofluorescence microscopy images of P1.HTR cells transfected with IDO1.WT, co-stained with antibodies recognizing IDO1 (green) and markers of intracellular organelles and structures (as indicated; red). Nuclei were stained with DAPI (blue). The merge imagine is shown for all stainings or without DAPI (no DAPI). Scale bar, 10 μm.

C   Immunoblotting analysis of EE purified from P1.IDO1.WT cells. Mock-transfected cells as in (A) were used as control.

D   Distribution of the IDO1.WT protein expressed by P1.HTR transfected cells in isopycnic sucrose gradients. Fractions were immunoblotted using antibodies specific for IDO1 and intracellular organelles or structures as indicated.

Data information: In all panels, one of three representative experiments is shown.
Source data are available online for this figure.

Figure 4. The YENM Motif is required for IDO1 EE localization in tumor transfectants.

A Confocal immunofluorescence microscopy images of P1.HTR cells transfected with IDO1.WT or IDO1.Y149F and co-stained with antibodies recognizing IDO1 (green) and EEA1 (red). Nuclei were stained with DAPI (blue). The merge imagine is shown for all stainings or without DAPI (no DAPI). Scale bar, 10 μm.

B Pearson's coefficient of IDO1 colocalization with EEA1 in P1.HTR cells transfected as in (A), with each point representing colocalization within an image stack. Data represent mean ± SD ($n >$ 24 cells from three independent experiments). Statistical analysis was performed using two-tailed unpaired Student's t-test. ***$P < 0.001$.

C Distribution of IDO1.WT and the IDO1.Y149F mutants in homogenates of P1.HTR cells along the isopycnic sucrose gradient as in Fig 3D. Fractions were immunoblotted using antibodies specific for IDO1.

D The distribution of IDO1.WT and IDO1.Y149F proteins along the isopycnic sucrose gradient is shown in term of densitometric analysis in each fraction (mean ± SD of three experiments).

Source data are available online for this figure.

(Fig 5D). In contrast, the inhibitors did not exert any significant effect on Kyn production by the same cells over 24 h of observation (Fig EV3). As mentioned above, the finding that TGX-221 only partially impaired the effects associated with IDO1 signaling may suggest that the inhibitor is not fully active in our setting. Overall, these data indicated that class IA PI3K p110 subunits are components of the p85/IDO1 complex and that their catalytic activity is required for IDO1 anchoring to EE and consequent partnership with tyrosine phosphatases.

The signaling form of IDO1 co-localizes with EE in pDCs

Because class IA PI3K p110 activity is involved in the IDO1 signaling pathway in pDCs (Fig 1) and in both signaling and IDO1 localization
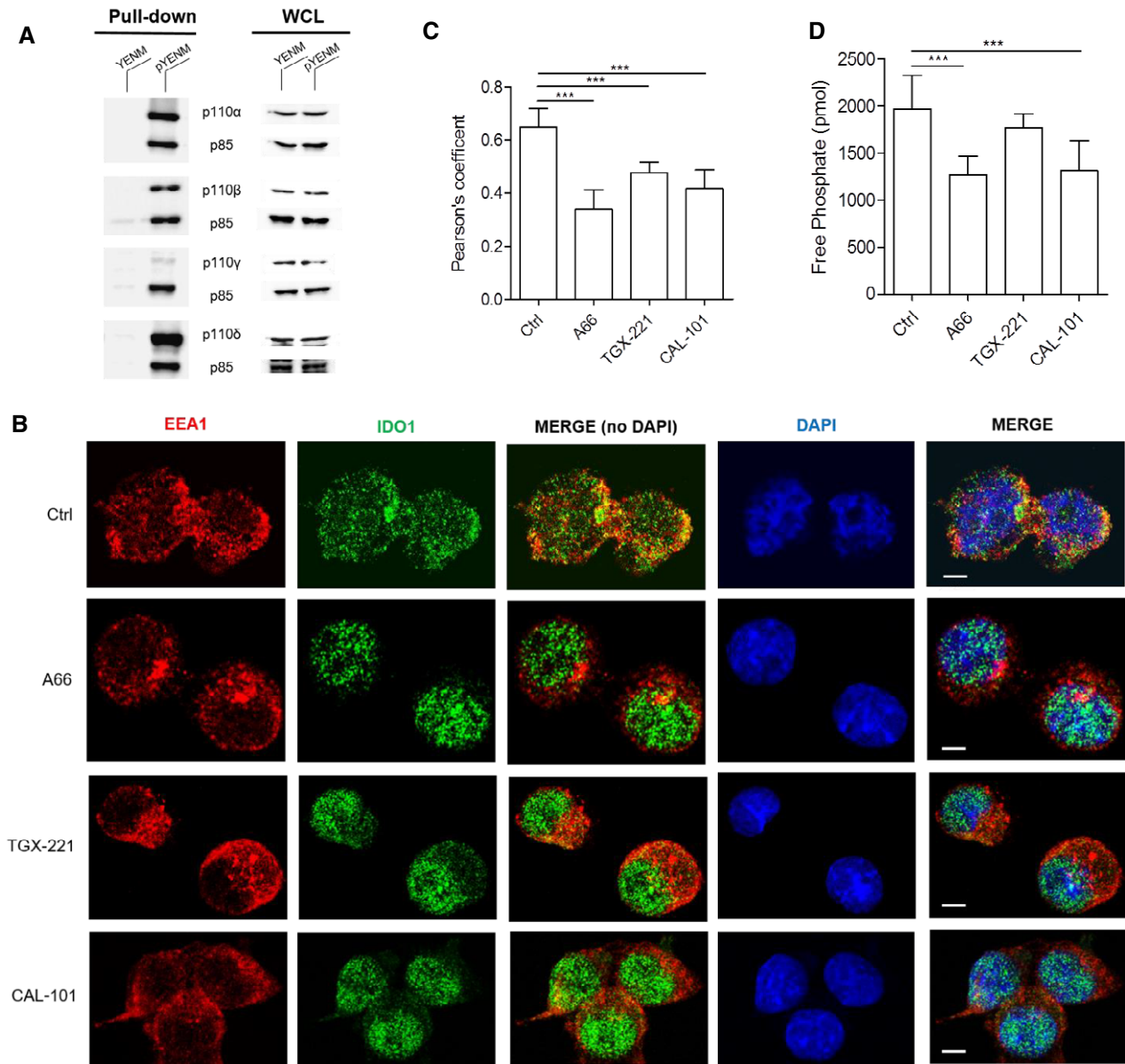
Figure 5. Class IA PI3K p110 activity is required for IDO1 signaling and EE localization in tumor transfectants.

A Pull-down assay of lysates from untransfected P1.HTR cells with unphosphorylated (YENM) and tyrosine-phosphorylated (pYENM) IDO1 peptides analyzed by immunoblotting with anti-p85, -p110α, -p110β, -p110γ, and -p110δ antibodies. Whole cell lysates (WCL) were used as control of lysate amount.

B Confocal immunofluorescence microscopy images of P1.HTR cells transfected with IDO1.WT incubated with class IA PI3K p110 isoform inhibitors (indicated) or medium alone (Ctrl) for 24 h and co-stained with antibodies recognizing IDO1 (green) and EEA1 (red). Nuclei were stained with DAPI (blue). The merge imagine is shown for all stainings or without DAPI (no DAPI). Scale bar, 10 μm.

C Pearson's coefficient of IDO1 colocalization with EEA1 in P1.HTR cells transfected and treated as in (B), with each point representing colocalization within an image stack. Data represent mean ± SD ($n > 20$ cells from two independent experiments).

D Tyrosine phosphatase activity in anti-IDO1 immunoprecipitates from P1.HTR cells transfected with IDO1.WT and treated with PI3K catalytic inhibitors (indicated) or medium alone (Ctrl). Data represent the mean ± SD ($n = 3$ technical replicates).

Data information: One of two (A) and three (B and D) representative experiments is shown. Statistical analysis was performed using ANOVA followed by post-hoc Bonferroni's test. ***$P < 0.001$.

Source data are available online for this figure.

to EE in tumor transfectants (Fig 5), we investigated whether the signaling form of IDO1 would localize to EE in pDCs as well, namely, cells physiologically exploiting IDO1 as an immunoregulatory mechanism. By using confocal microscopy following immunostaining with an IDO1-specific antibody, we investigated the cellular topology of IDO1 in freshly purified pDCs stimulated for 24 h with either IFN-γ, a stimulant of the catalytic form, or TGF-β, which fosters the signaling activity (Pallotta *et al*, 2011; Pallotta

et al, 2014; Mondanelli et al, 2017a). pDCs incubated with medium alone were used as a control. Antibodies recognizing specific markers of organelles and DAPI staining were used as in Fig 3B. In accordance with previous data (Pallotta et al, 2011; Pallotta et al, 2014), pDCs did express IDO1 in the absence of external stimuli (Fig 6A), although to a lesser extent as compared to conditioning with TGF-β and more so, with IFN-γ (Figs 6B and C). IDO1 staining in unconditioned cells appeared both diffuse and concentrated in discrete spots, similarly to P1.HTR cells transfected with IDO1.WT (Figs 3A and B). Lack of co-staining with anti-calnexin, anti-TGN-38, and DAPI excluded localization of the IDO1 protein in the endoplasmic reticulum, Golgi apparatus, and nucleus, respectively (Fig 6A). In contrast, a merge analysis of IDO1 and EEA1 or LAMP1 indicated that the few IDO1 hotspots detectable in untreated pDCs co-localized with EE and, at least in part, with lysosomes (Fig 6A). Perhaps more importantly, pDC conditioning with IFN-γ led to the exclusion of IDO1 from EEA1-expressing subcellular structures, whereas EE co-localization of the IDO1 protein greatly increased in TGF-β−treated pDCs (Fig 6B and C).

Therefore, these data suggested that in primary splenic pDCs, IDO1 is basally expressed in both cytosol and EE. In line with its aptitude to induce the formation of EE acting as signaling platforms (Derynck & Zhang, 2003), TGF-β appeared to be a favorable stimulus in shifting IDO1 proteins from cytosol to the small organelles (Fig 7), an event likely occurring also in unstimulated DCs, as a result of their basal production of TGF-β (Mondanelli et al, 2017a), and in P1.HTR cells, which produce considerable levels of the cytokine (Fig EV4).

Discussion

Signal transduction involves the transmission of a signal in time and space. Because proteins cannot diffuse as quickly as small-molecule second messengers, the subcellular localization of signaling proteins is a key element of many signal transduction circuits (Hung & Link, 2011). Thus, knowledge of the spatial distribution of signaling proteins at the subcellular level is key to an understanding of a protein's function(s) and to optimizing drug development.

IDO1 is an eclectic enzyme endowed with catalytic and signaling functions, both responsible for immunoregulatory effects in health and disease (Mondanelli et al, 2017b, Orabona et al, 2018, Mondanelli et al., 2019b). IDO1 catalytic activity is more intense but transient (Pallotta et al, 2011) and is known to reside in the cytosol of cells, including DCs and tumor cells. IDO1, in fact, constitutes the target of several experimental anti-tumor drugs (Mondanelli et al, 2017b). Although IDO1 catalytic inhibitors can effectively enhance anti-tumor immune responses—at least in preclinical models (Prendergast et al, 2018)—one of these drugs, i.e., epacadostat, recently showed poor efficacy in cancer patients in combination with pembrolizumab, an anti-PD-1 antibody (Garber, 2018). As a consequence of this failure, other clinical trials with IDO1 inhibitors have been suspended, canceled, or downsized. Although several reasons may explain epacadostat's results, lack of consideration of IDO1 signaling activity could have played an important role (Albini et al, 2018).

We here found that the IDO1 signaling form does not reside in the cytosol but rather in EE, a location "legitimated" for hosting

intracellular signaling platforms (Murphy et al, 2009), including those of the TGF-β receptor (Derynck & Zhang, 2003), whose activation triggers the IDO1 signaling pathway. Moreover, anchoring to EE required the partnership with, and activation of, class IA PI3K subunits.

In EE, IDO1 appeared to be tyrosine-phosphorylated in its ITIMs, an event necessary for direct interaction with and activation of SHPs, activation of the noncanonical NF-κB pathway, and upregulation of both IDO1 and TGF-β encoding genes (Pallotta et al, 2011; Pallotta et al, 2014; Mondanelli et al, 2017a). In pDCs as well as in transfected tumor cells, a discrete amount of IDO1 localized in EE was detected in unstimulated, homeostatic conditions. These data could be explained by the fact that both types of cell produce TGF-β, which could act in an autocrine/paracrine fashion (Mondanelli et al, 2017a) to promote the formation of endocytic vesicles as well as the activation of PI3K (Derynck & Zhang, 2003), which effects are both required for the IDO1 signaling pathway. However, it should be considered that, in unstimulated human ovarian cancer cells, IDO1 is dynamically bound to its heme cofactor and, perhaps more importantly, at least 85% of IDO1 occurs in the apo-form, i.e., catalytically inactive, that can nevertheless be activated by exogenously added heme (Nelp et al, 2018). Moreover, de novo heme synthesis is required for induction of the active IDO1 enzyme in IFN-γ–stimulated, human monocyte-derived macrophages (Thomas et al, 2001). Therefore, in the absence of exogenous signals, IDO1 occurs in the cell as a "pool" of different proteins, which can be distinguished by the presence of heme, phosphorylation, and topology. Although uninvestigated as yet, the novel catalytic inhibitors that bind IDO1 in its apo-form (Nelp et al, 2018) may also influence IDO1 localization in EE. In the presence of specific signals, the IDO1 molecules of the initial pool could be extensively modified (i.e., by heme incorporation for catalytic activity or phosphorylation of YENM for signaling) and thus directed to perform a unique role, catalytic or signaling at either the cytosolic or EE site, respectively, depending on the nature of the signal.

Initially considered only a switch to promote cellular activation, the PI3K signaling pathway has been recognized as an important player in orchestrating both pro-inflammatory and anti-inflammatory mechanisms to maintain effective immunity while protecting host tissues. This is accomplished by activation of downstream effectors such as Akt and also by escorting target proteins to specific subcellular compartments. However, only recently has the role—either pro- or anti-inflammatory—of each PI3K member begun to be clarified, thanks to the availability of selective inhibitors and knockout mice for the PI3K p110 isoforms (Stark et al, 2015). An interest has thus been increasing in the PI3K p110δ subunit, largely restricted to the immune system. This subunit greatly influences the signaling of Toll-like receptor 4, by directing its transit from the plasma membrane to EE and thus favoring an anti-inflammatory pathway in cDCs that protects mice from endotoxic shock (Aksoy et al, 2012). Interestingly, cDCs expressing IDO1, phosphorylated in its ITIMs and thus capable of signaling activity, protect mice from endotoxin shock (Bessede et al, 2014) and neuroinflammation (Volpi et al, 2016). Moreover, disrupted PI3K p110δ dysregulates maternal immune tolerance and increases fetal mortality in mice, an effect mainly due to the induction of hyper-inflammatory macrophages (Kieckbusch et al, 2015). Although we do not know whether the IDO1 signaling plays any
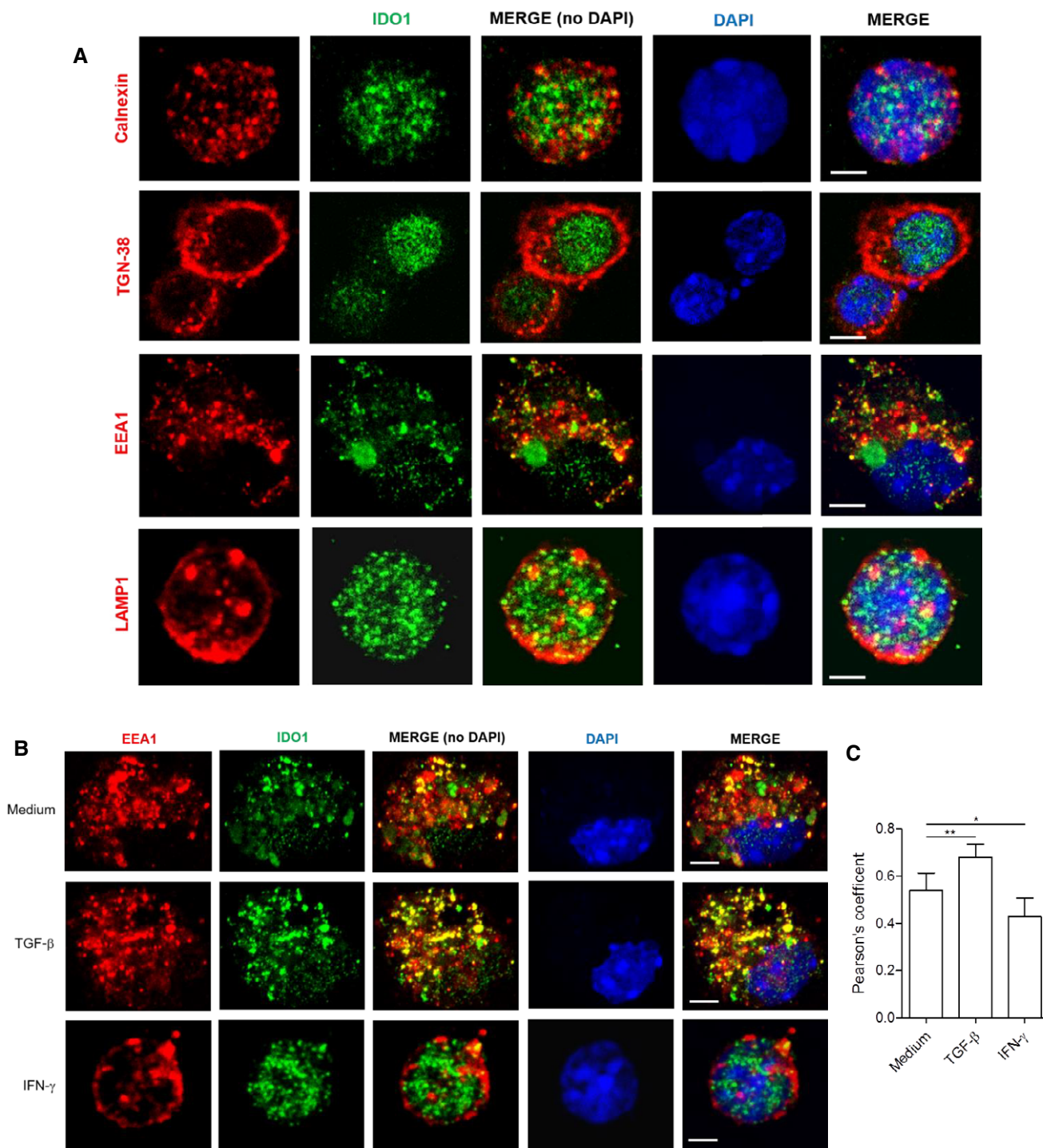
Figure 6. The signaling but not catalytic form of IDO1 colocalizes with EE in pDCs.

A Confocal immunofluorescence microscopy images of freshly purified pDCs co-stained with antibodies recognizing IDO1 (green) and markers of intracellular organelles and structures (indicated; red). Nuclei were stained with DAPI (blue). The merge imagine is shown for all stainings or without DAPI (no DAPI). Scale bar, 5 μm.

B Confocal immunofluorescence microscopy images of pDCs incubated for 24 h with TGF-β or IFN-γ and co-stained with antibodies recognizing IDO1 (green) and EEA1 (red). Nuclei were stained with DAPI (blue). Scale bar, 5 μm.

C Pearson's coefficient of IDO1 colocalization with EEA1 in pDCs either untreated or stimulated with TGF-β or IFN-γ (as in B), with each point representing colocalization within an image stack. Data represent mean ± SD ($n >$ 20 cells from three independent experiments).

Data information: In (A and B), one representative experiment of three is shown. Statistical analysis was performed using ANOVA followed by post-hoc Bonferroni's test. *$P < 0.05$; **$P < 0.01$.
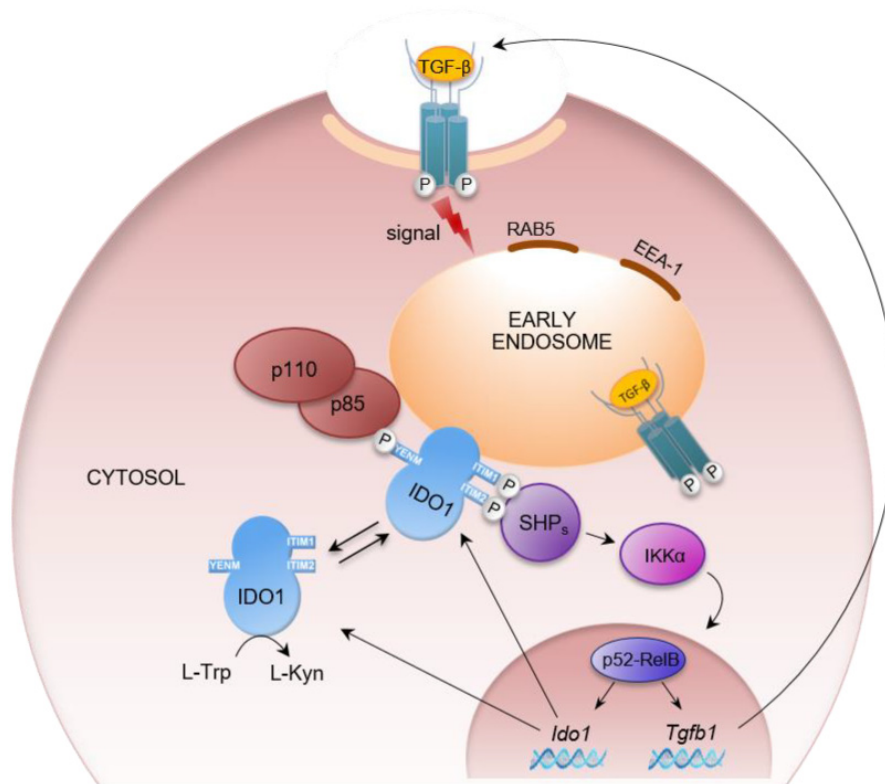
Figure 7. Scheme of the possible role of the class IA PI3Ks in the overall immunoregulatory IDO1 signaling pathway in pDCs.

roles, mouse and human placental cells do express high levels of IDO1 (Mellor *et al*, 2001; Theate *et al*, 2015), which is required for the maintenance of maternal T cell tolerance in mice (Munn *et al*, 1998). In addition, although stimuli other than TGF-β can trigger IDO1's signaling, the cytokine, via PI3K, appears to be an obligate endogenous mediator for the perpetuation of the IDO1 pathway, at least in pDCs (Volpi *et al*, 2013; Volpi *et al*, 2016; Mondanelli *et al*, 2017a).

PI3Ks now stand out among several signaling pathways as promising drug target for immune-related disorders and cancer as well (Stark *et al*, 2015). In neoplastic conditions, activation of PI3K p110δ can indeed induce proliferation and survival of tumor cells as well as potentiation of immunoregulatory mechanisms in both tumor and immune cells, thus dampening anti-tumor immunity (Dong *et al*, 2019). However, in great part, these effects are indirect, i.e., due to the influence of subcellular translocation and thus the function of selected downstream protein targets, including IDO1, as it is suggested by the present study. In addition, p110α, the alternative class IA PI3K isoform involved in IDO1 signaling and immunoregulatory effects, is the only PI3K gene found to be mutated in cancer (Vanhaesebroeck *et al*, 2010). Very recently, kynurenines were found to activate the class IA PI3K-Akt pathway in neoplastic colon epithelium, suggesting the existence of a bidirectional link between the two pathways (Bishnupuri *et al*, 2019). Therefore, co-administration of class IA PI3K selective inhibitors may increase the rate of success of effective therapeutic targeting of IDO1 in neoplasia.

Materials and Methods

Mice and cell lines

Eight- to ten-week-old female C57BL/6 mice were obtained from Charles River Breeding Laboratories and used for pharmacological studies. The *in vivo* experiments performed with wild-type C57/BL6 mice were approved by the Italian Ministry of Health. p110α$^{D933A/WT}$, p110δ$^{D910A/D910A}$, and p110γ^{KO} mice were bred at the Bellvitge Biomedical Research Institute (IDIBELL), University of Cambridge, and Babraham Institute, respectively. Mice were kept in individually ventilated cages and cared for according to the guidelines and legislation of Spain and United Kingdom. All knock-in and knockout mice were backcrossed onto the C57/BL6 background for > 10 generations, and wild-type littermates were used as controls. Spleens of knock-in and knockout mice and relative controls were sent to the Dept. of Experimental Medicine, University of Perugia, where pDCs were purified and analyzed. All mice bearing the correct genotype were enrolled sequentially; therefore, randomization was not applicable. Mice with animal welfare issues in the absence of any treatment were excluded from the study. For all experiments involving only wild-type animals, randomization was applied. P1.HTR, a highly transfectable clonal variant of mouse mastocytoma P815 (Albini *et al*, 2017), was cultured in Iscove's modified Dulbecco's medium supplemented with 10% FCS at 37°C and routinely tested for mycoplasma contamination.

Purification and cell treatment of DCs

All purification procedures of pDCs and CD8^{−} cDCs from mouse spleens have been described (Grohmann *et al*, 2007; Pallotta *et al*, 2011; Mondanelli *et al*, 2017a). The pDCs were exposed for 24 h at 37°C to IFN-γ (100 ng/ml; Peprotech) or TGF-β (20 ng/ml; R&D Systems). Blockers of p110 isoform activity were added at 100 nM 1 h before cytokine treatment and left in culture for the remaining 24 h (A66, TGX-221, CAL-101, and LY294002; MedChemExpress). The concentration used for all compounds (100 nM) was tested for cell toxicity in both pDCs and P1 cells and none was found. The choice of this concentration was based on the known IC_{50} values toward the intended target isoform versus others. More specifically, for A66, the reported IC_{50} for p110α is 32 nM, p110β > 12,500 nM, p110δ > 1,250 nM, and p110γ 3,480 nM (Jamieson *et al*, 2011). Therefore, the concentration of 100 nM was far below the concentrations required to inhibit the other PI3K isoforms and, at the same time, approximately three times the IC_{50} for p110α (that might contain the possible variables occurring between cell-free assays and by using specific types of cells). For TGX-221, the concentration of 100 nM was the same used previously (Foukas *et al*, 2006). However, although displaying an IC_{50} of 5 nM for p110β, 5,000 nM for p110α, and ≥ 3,500 nM for p110γ, the IC_{50} of TGX-221 for p110δ has been reported to be 100 nM. Therefore, we cannot exclude that, in our conditions, TGX-221 could have also inhibited p110δ, the PI3K catalytic isoform that appears to better associate with the p85/IDO1 complex (Fig. 5A). Nevertheless, in a previous study (Jackson *et al*, 2005), PI3K p110δ-deficient mouse platelets were sensitive to the effects of TGX-221 (used at the concentration of 500 nM) as wild-type cells, suggesting that, at least in platelets, TGX-221 does not inhibit the p110δ subunit. For CAL-101, the IC_{50} for p110δ is 2.5 nM, p110γ 89 nM, p110β i565 nM, and for p110α 820 nM (Lannutti *et al*, 2011) (Lannutti *et al*, 2011). Therefore, this profile would suggest that CAL-101 at 100 nM can inhibit both p110δ and p110γ, as indicated in Fig 1B.

Transfection of pDCs with PI3K p110α-, β-, and δ-specific siRNA was done as described (Grohmann *et al*, 2007; Pallotta *et al*, 2011; Pallotta *et al*, 2014). Gene-specific siRNAs were predesigned by Ambion, which also supplied negative control siRNA.

Generation and expression of *Ido1* gene constructs

The construct expressing wild-type (WT) *Ido1* was generated from cDNA of splenic mouse cDCs stimulated with IFN-γ, as previously described (Pallotta *et al*, 2011; Albini *et al*, 2017). The Y149F *Ido1* mutant was obtained by means of crossover PCR with primers containing specific substitutions, as described (Pallotta *et al*, 2011; Albini *et al*, 2017). For both WT and mutated *Ido1* constructs, 20 μg DNA was used to transfect 1×10^7 P1.HTR cells by electroporation and stable transfectants were obtained by puromycin selection. P1.HTR cells, either untransfected or stably transfected with the empty plasmid (mock), were used as control.

Confocal microscopy and image processing and quantification

Confocal images were captured by means of an LSM800 Airyscan laser confocal microscope (Zeiss) equipped with laser emission lines at 458, 488, 543, and 633 nm, using a Plan-Apocromat 63X/1.40 NA objective with oil immersion. Images were analyzed and recorded by using a Zeiss imaging software (Zeiss) and collected by means of 488-nm (for Alexa Fluor 488-conjugated goat anti-rabbit IgG; Thermo Fisher Scientific), 678-nm (for Alexa Fluor 647-conjugated anti-mouse IgG; Thermo Fisher Scientific), and 357-nm (for DAPI) laser lines for excitation. Acousto-optic tunable filter-controlled tuning of laser lines, pinhole diameters, and light collection configuration were optimized to obtain best signal-to-noise ratio and to avoid fluorescence crossover. Images were acquired at the resolution of 1,024 × 1,024 pixels (image size) and 8 bit. Quantification of the co-localization of the two-three (when DAPI was also included) fluorophores was performed using ImageJ with the Jacob plug-in and expressed in terms of Pearson's coefficient (ranging from −1, i.e., negative correlation, to +1, complete positive correlation) (Adler & Parmryd, 2010). For IDO1 staining, a specific rabbit polyclonal antibody (CV152) developed in our laboratory was used (Romani *et al*, 2008). Other primary antibodies were from Santa Cruz Biotechnology (anti-EEA1, clone G-4 Cat# sc-137130; anti-LAMP1, clone E-5 Cat# sc-177768; Anti-TGN38 clone G-9 Cat# sc-271624) and Thermo Fisher Scientific (anti-calnexin, clone AF18 Cat# MA3-027).

Real-Time PCR

Real-Time RT–PCR (for mouse *Ido1*, *Tgfb1*, and *Gapdh*) analyses were carried out as described (Pallotta *et al*, 2011; Mondanelli *et al*, 2017a). Data were calculated as the ratio of gene to *Gapdh* expression by the relative quantification method ($\Delta\Delta C_T$; means ± SD of triplicate determination), and data are presented as normalized transcript expression in the samples relative to normalized transcript expression in control cultures (in which fold change = 1; dotted line).

Kynurenine and phosphatase assays

IDO1 functional activity was measured in culture supernatants in terms of the ability to metabolize L-tryptophan to Kyn, whose concentrations were measured by high-performance liquid chromatography in 24 h culture supernatants after the addition of 100 μM L-tryptophan for the final 8 h for pDCs but not tumor cell transfectants (Fallarino *et al*, 2003; Grohmann *et al*, 2007). To measure the tyrosine phosphatase activity associated with IDO1 co-immunoprecipitates, the dephosphorylation of peptides with phosphorylated tyrosine residues was assayed by using a phosphatase assay kit (Tyrosine Phosphatase Assay System) according to the manufacturer's procedure (Promega) and as described (Pallotta *et al*, 2011; Albini *et al*, 2017; Albini *et al*, 2018). Because reliable measurements of tyrosine phosphatase activity co-precipitated with IDO1 would require a high number of cells and IDO1 expression, we evaluated the activation of the IDO1 signaling pathway in pDCs by means of the sensitive technique of Real-Time PCR to quantify the induction of *Ido1* and *Tgfb1* gene expression, the downstream effects of IDO1 signaling (Pallotta *et al*, 2011; Bessede *et al*, 2014; Pallotta *et al*, 2014; Albini *et al*, 2018).

Isopycnic gradient analysis

Subcellular fractionation was performed by isopycnic gradient ultracentrifugation as described (De Marchis *et al*, 2018). Briefly, cells were homogenized with buffer without detergent (12% sucrose,

10 mM KCl, 2 mM MgCl$_2$, 100 mM Tris–HCl, pH 7.8). One ml of homogenate was loaded on the top of a 16–55% (w/w) continuous sucrose gradient. After ultracentrifugation at 141,000 g for 4 h at 4 °C, 15 fractions of one ml each were collected starting from the top of each gradient. An equal aliquot of each fraction (usually 40 μl) was separated by SDS–PAGE and then analyzed by immunoblotting with the anti-IDO1 antibody. Anti-EEA1 (rabbit mAb clone C45B10 Cat# C45B10), anti-Golgin97 (clone rabbit mAb D8P2K Cat# 13192); anti-LAMP1 (rabbit mAb clone C54H11 Cat# 3243), and anti-calreticulin (rabbit mAb clone D3E6 Cat# 12238) antibodies were from Cell Signaling Technology. Relative protein expression was quantified by using an ImageQuant TL LAS4000 mini densitometer and the Analysis Toolbox software (GE Healthcare). Densitometric analysis of the specific signals was performed within a linear range of exposure of the blots, selecting in each experiment the two lowest exposure times useful to detect the signals, as described (Albini *et al*, 2017; Gargaro *et al*, 2019).

Purification of endosomes

Endosome purification was performed as described (Castellino & Germain, 1995). Briefly, 2×10^8 P1 tumor cells, either transfected with the empty vector or IDO1.WT, were washed repeatedly in PBS and resuspended in PBS containing 0.25 M sucrose and 2 mM HEPES (pH 7.4). Cells were homogenized in a Dounce homogenizer and spun at 150 g for 10 min at 4°C. The supernatant was loaded onto a 27% percoll gradient laid over a 0.25 M sucrose cushion and centrifuged for 1 h at 34,000 g at 4°C. The band at the interface was enriched in late and early endosomes and was further separated on a 10% percoll gradient by centrifugation at 34,000 g for 1 h. Purity of the early endosome fraction was confirmed by the presence and absence of Rab5 and Rab7, respectively (Fig 2C), by using anti-Rab5 (rabbit mAb clone C8B1 Cat# 3547) and anti-Rab7 (rabbit mAb clone D95F2 Cat #9367), both from Cell Signaling Technology.

Immunoprecipitation, pull-down analysis, and Western blotting

These procedures were done as described (Orabona *et al*, 2008). For immunoprecipitation of IDO1, a rabbit monoclonal anti-mouse IDO1 antibody (CV152) obtained in our laboratory (Pallotta *et al*, 2011) was used. The following peptides were used for pull-down experiments: biotinylated phosphorylated ITIM1 (SGSGNIAVPpY115CELSE; Genosys-Sigma), biotinylated phosphorylated ITIM2 (SGSGPEGLL-pY254EGVWD; Genosys-Sigma), and biotinylated unphosphorylated (SGSGPMTY149ENMDI) and phosphorylated YENM (SGSGPMTpY149ENMDI; both from Genemed Synthesis). Antibodies used to analyze pull-down and immunoprecipitated samples were SH-PTP1 (clone C-19 Cat# sc-287) and SH-PTP2 (clone B-1 Cat #sc-7384), both from Santa Cruz Biotechnology. PI3K p85 (rabbit mAb clone 19H8 Cat #42575), p110α (rabbit mAb clone C73F8 Cat #4249), p110β (rabbit mAb clone C33D4 Cat #3011), p110γ (rabbit mAb clone D55D5 Cat #5405), and p110δ (rabbit clone D1Q7R Cat #34050) antibodies were from Cell Signaling Technology.

Multiple sequence alignment

IDO1 sequences for *M. musculus* (sp|P28776|I23O1_MOUSE), *R. norvegicus* (sp|Q9ERD9|I23O1_RAT), and *H. sapiens* (sp|P14902|I23O1_HUMAN) as well as IDO2 sequences for *H. sapiens* (sp|Q6ZQW0|I23O2_HUMAN), *M. musculus* (sp|Q8R0V5|I23O2_MOUSE), and *R. norvegicus* (sp|F1LV46|I23O2_RAT) were obtained from UniProt (https://www.uniprot.org/). The IDO1 sequence for *C. lupus dingo* (XP_025293004.1) and the IDO2 sequences for *D. rerio* (XP_021333978.1) and *G. gallus* (XP_424397.3) were obtained from the NCBI Protein database (https://www.ncbi.nlm.nih.gov/protein). Multiple sequence alignment was performed using Clustal Omega (https://www.ebi.ac.uk/Tools/msa/clustalo/) with default parameters and visualized using Unipro UGENE (http://ugene.net/).

Molecular modeling

The crystal structure of IDO1 in complex with L-Trp (pdb code, 5WMU) and the structure of the SH2 domain of PI3K p85 (pdb code, 1H9O) were taken from the protein database (Bernstein *et al*, 1977). A protein–protein docking study was then performed using ClusPro web-based server (https://cluspro.org) (Kozakov *et al*, 2017). ClusPro uses a rigid body docking procedure with PIPER algorithm to sample billions of conformations (Kozakov *et al*, 2006). A number of 1,000 lowest energy structures was generated and clustered using root-mean-square deviation (RMSD). Geometries of selected complexes were refined using energy minimization. We used the van der Waals + electrostatic scoring scheme, as implemented in PIPER, to assess the interaction energy between IDO1 and the SH2 domain of PI3K p85. The top ten most populated clusters (Table EV1, clusters n. 0–9) were visually inspected searching for solutions close to the expected native structure of the complex, in which the protein–protein interaction interface is likely constituted by the YENM motif of IDO1 and the phosphotyrosine binding site of the SH2 domain of PI3K p85. As a result, six out of ten clusters (cluster n. 0, 1, 3, 5, 6, 8) displayed models with the interface close to the expected native structure of the complex (Fig EV5), with model of cluster n. 8 being the closest to the native structure in terms of distance between the YENM motif of IDO1 and the phosphotyrosine binding site of the SH2 domain in p85. Images of IDO1/p85 SH2 domain complex were made with VMD (VMD is developed with NIH support by the Theoretical and Computational Biophysics group at the Beckman Institute, University of Illinois at Urbana-Champaign). Solvent accessible surface areas (SASA) were calculated on tyrosine residues of YENM motif and YITM motif and reported as average ± SD of relative SASA values obtained from each chain of available IDO1 crystal structures (Y149 = 25.3 ± 9.6 Å2; Y89 = 5.5 ± 2.8 Å2; n.106 chain structures). Maximum values found for Y149 and Y89 in specific chain structures were also calculated (Y89 max value = 16.0 Å2 in the crystal structure 6R63; Y149 max value = 49.2 Å2 in the crystal structure 6E44). Calculations of SASA were performed using Gromacs (v.5.1.5).

Analysis of pDC gene expression data

Gene expression data of pDCs, obtained using Mouse Gene 1.0 ST (GSM605840, GSM605841, GSM605842, GSM605843, GSM605844, GSM605845, GSM854297, GSM854298) and Mouse Genome 430 2.0 (GSM247591, GSM247592, GSM461452, GSM461453) arrays were downloaded from Gene Expression Omnibus. For each type of microarray, fluorescence signals were background-adjusted, normalized using quantile normalization and expression values calculated

using median polish summarization (*rma* function of *affy* Bioconductor package) and BrainArray chip definition files (CDF) for mouse 1.0 ST and 430 2.0 arrays based on Entrez Gene IDs (http://brainarray.mbni.med.umich.edu/Brainarray/Database/CustomCDF/21.0.0/entrezg.asp; version 21.0.0). The two sets of expression data have been merged matching the 16,804 common Entrez Gene IDs of the 1.0 ST and 430 2.0 custom CDFs. A direct merging of raw fluorescence signals (i.e., of CEL files), although desirable for an optimal removal of batch effects, was unfeasible due to the different probe sequences synthesized on the 1.0 ST and 430 2.0 microarrays. Consequently, batch effects have been removed applying the *ComBat* function of the *sva* Bioconductor package to the merged matrix. *ComBat* was used with default parameters with the exception of the adjustment variables that were imputed as a vector of array type labels. All data analyses were performed in R 3.4.4 (The Comprehensive R Archive Network).

Skin test assay

A skin test assay was used for measurements of major histocompatibility complex class I–restricted delayed-type hypersensitivity (DTH) responses to the HY peptide in C57BL/6 female recipient mice, as described (Puccetti *et al*, 1994; Grohmann *et al*, 2002; Grohmann *et al*, 2007; Pallotta *et al*, 2011; Mondanelli *et al*, 2017a). For *in vivo* immunization, 3×10^5 peptide-loaded $CD8^-$ cDCs, combined with a minority fraction (5%) of peptide-loaded C57BL/6 pDCs, were injected i.p. into recipient mice. Two weeks later, a DTH response was measured to intrafootpad challenge with the eliciting peptide, and results were expressed as the increase in footpad weight of peptide-injected footpads over that of vehicle-injected (internal control) counterparts. Measurements were performed in a blinded fashion. The minority cell fraction, constituted by pDCs, was left untreated or treated overnight with specific reagents as described above.

Statistical analysis

All analyses were performed using Prism version 6.0 (GraphPad Software). Data usually met normality and were analyzed by two-tailed unpaired Student's *t*-test or ANOVA followed by post-hoc Bonferroni's test, when three or more samples were under comparison, respectively. Alternatively, the nonparametric Mann–Whitney test or Kruskal–Wallis with post-hoc Dunn's test was used. A *P* value less than 0.05 was considered significant. Overall results, obtained by at least three replicates per experimental parameter, were shown as mean ± SD. For the skin test assay, the paired Student's *t*-test was used (using at least six mice per group, as computed by power analysis to yield a power of at least 80% with and α-value of 0.05).

Data availability

No primary datasets have been generated or deposited.

Expanded View for this article is available online.

Author contributions

Conceptualization, MTP and UG; Methodology, FM, SB, MB, and AM; Investigation, MTP, AI, AP, FDM, EPa, FAG, AC, CO, CVo, MLB, GM, EA, CVa, MG, FF, RB, CDML, EMCM, EPr, and IMI; Writing & Editing, UG and PP; Funding acquisition, UG, AM, and MTP; Resources, MPM, MGG-M, JLS, PH, SS, KO, A-KS, FG and LS; Supervision, UG.

Conflict of interest

The authors declare that they have no conflict of interest.

References

Adler J, Parmryd I (2010) Quantifying colocalization by correlation: the Pearson correlation coefficient is superior to the Mander's overlap coefficient. *Cytometry Part A* 77: 733–742

Aksoy E, Taboubi S, Torres D, Delbauve S, Hachani A, Whitehead MA, Pearce WP, Berenjeno IM, Nock G, Filloux A *et al* (2012) The p110delta isoform of the kinase PI(3)K controls the subcellular compartmentalization of TLR4 signaling and protects from endotoxic shock. *Nat Immunol* 13: 1045–1054

Albini E, Coletti A, Greco F, Pallotta MT, Mondanelli G, Gargaro M, Belladonna ML, Volpi C, Bianchi R, Grohmann U *et al* (2018) Identification of a 2-propanol analogue modulating the non-enzymatic function of indoleamine 2,3-dioxygenase 1. *Biochem Pharmacol* 158: 286–297

Albini E, Rosini V, Gargaro M, Mondanelli G, Belladonna ML, Pallotta MT, Volpi C, Fallarino F, Macchiarulo A, Antognelli C *et al* (2017) Distinct roles of immunoreceptor tyrosine-based motifs in immunosuppressive indoleamine 2,3-dioxygenase 1. *J Cell Mol Med* 21: 165–176

Ball HJ, Sanchez-Perez A, Weiser S, Austin CJ, Astelbauer F, Miu J, McQuillan JA, Stocker R, Jermiin LS, Hunt NH (2007) Characterization of an indoleamine 2,3-dioxygenase-like protein found in humans and mice. *Gene* 396: 203–213

Bernstein FC, Koetzle TF, Williams GJ, Meyer Jr EF, Brice MD, Rodgers JR, Kennard O, Shimanouchi T, Tasumi M (1977) The Protein Data Bank: a computer-based archival file for macromolecular structures. *J Mol Biol* 112: 535–542

Bessede A, Gargaro M, Pallotta MT, Matino D, Servillo G, Brunacci C, Bicciato S, Mazza EM, Macchiarulo A, Vacca C *et al* (2014) Aryl hydrocarbon receptor control of a disease tolerance defence pathway. *Nature* 511: 184–190

Bishnupuri KS, Alvarado DM, Khouri AN, Shabsovich M, Chen B, Dieckgraefe BK, Ciorba MA (2019) IDO1 and Kynurenine Pathway Metabolites Activate PI3K-Akt Signaling in the Neoplastic Colon Epithelium to Promote Cancer Cell Proliferation and Inhibit Apoptosis. *Cancer Res* 79: 1138–1150

Black DL (2000) Protein diversity from alternative splicing: a challenge for bioinformatics and post-genome biology. *Cell* 103: 367–370

Castellino F, Germain RN (1995) Extensive trafficking of MHC class II-invariant chain complexes in the endocytic pathway and appearance of peptide-loaded class II in multiple compartments. *Immunity* 2: 73–88

Chuang E, Fisher TS, Morgan RW, Robbins MD, Duerr JM, Vander Heiden MG, Gardner JP, Hambor JE, Neveu MJ, Thompson CB (2000) The CD28 and CTLA-4 receptors associate with the serine/threonine phosphatase PP2A. *Immunity* 13: 313–322

De Marchis F, Colanero S, Klein EM, Mainieri D, Prota VM, Bellucci M, Pagliuca G, Zironi E, Gazzotti T, Vitale A *et al* (2018) Expression of

CLAVATA3 fusions indicates rapid intracellular processing and a role of ERAD. *Plant Sci* 271: 67–80

Derynck R, Zhang YE (2003) Smad-dependent and Smad-independent pathways in TGF-beta family signalling. *Nature* 425: 577–584

Dong S, Harrington BK, Hu EY, Greene JT, Lehman AM, Tran M, Wasmuth RL, Long M, Muthusamy N, Brown JR *et al* (2019) PI3K p110delta inactivation antagonizes chronic lymphocytic leukemia and reverses T cell immune suppression. *J Clin Investig* 129: 122–136

Engelman JA, Luo J, Cantley LC (2006) The evolution of phosphatidylinositol 3-kinases as regulators of growth and metabolism. *Nat Rev Genet* 7: 606–619

Fallarino F, Grohmann U, Hwang KW, Orabona C, Vacca C, Bianchi R, Belladonna ML, Fioretti MC, Alegre ML, Puccetti P (2003) Modulation of tryptophan catabolism by regulatory T cells. *Nat Immunol* 4: 1206–1212

Fallarino F, Grohmann U, Vacca C, Bianchi R, Orabona C, Spreca A, Fioretti MC, Puccetti P (2002) T cell apoptosis by tryptophan catabolism. *Cell Death Differ* 9: 1069–1077

Fallarino F, Grohmann U, You S, McGrath BC, Cavener DR, Vacca C, Orabona C, Bianchi R, Belladonna ML, Volpi C *et al* (2006) The combined effects of tryptophan starvation and tryptophan catabolites down-regulate T cell receptor zeta-chain and induce a regulatory phenotype in naive T cells. *J Immunol* 176: 6752–6761

Foukas LC, Claret M, Pearce W, Okkenhaug K, Meek S, Peskett E, Sancho S, Smith AJ, Withers DJ, Vanhaesebroeck B (2006) Critical role for the p110alpha phosphoinositide-3-OH kinase in growth and metabolic regulation. *Nature* 441: 366–370

Garber K (2018) A new cancer immunotherapy suffers a setback. *Science* 360: 588

Gargaro M, Vacca C, Massari S, Scalisi G, Manni G, Mondanelli G, Mazza EMC, Bicciato S, Pallotta MT, Orabona C *et al* (2019) Engagement of Nuclear Coactivator 7 by 3-Hydroxyanthranilic Acid Enhances Activation of Aryl Hydrocarbon Receptor in Immunoregulatory Dendritic Cells. *Front Immunol* 10: 1973

Geering B, Cutillas PR, Nock G, Gharbi SI, Vanhaesebroeck B (2007) Class IA phosphoinositide 3-kinases are obligate p85–p110 heterodimers. *Proc Natl Acad Sci USA* 104: 7809–7814

Grohmann U, Bianchi R, Orabona C, Fallarino F, Vacca C, Micheletti A, Fioretti MC, Puccetti P (2003a) Functional plasticity of dendritic cell subsets as mediated by CD40 versus B7 activation. *J Immunol* 171: 2581–2587

Grohmann U, Bronte V (2010) Control of immune response by amino acid metabolism. *Immunol Rev* 236: 243–264

Grohmann U, Fallarino F, Puccetti P (2003b) Tolerance, DCs and tryptophan: much ado about IDO. *Trends Immunol* 24: 242–248

Grohmann U, Mondanelli G, Belladonna ML, Orabona C, Pallotta MT, Iacono A, Puccetti P, Volpi C (2017) Amino-acid sensing and degrading pathways in immune regulation. *Cytokine Growth Factor Rev* 35: 37–45

Grohmann U, Orabona C, Fallarino F, Vacca C, Calcinaro F, Falorni A, Candeloro P, Belladonna ML, Bianchi R, Fioretti MC *et al* (2002) CTLA-4-Ig regulates tryptophan catabolism in vivo. *Nat Immunol* 3: 1097–1101

Grohmann U, Volpi C, Fallarino F, Bozza S, Bianchi R, Vacca C, Orabona C, Belladonna ML, Ayroldi E, Nocentini G *et al* (2007) Reverse signaling through GITR ligand enables dexamethasone to activate IDO in allergy. *Nat Med* 13: 579–586

Honig A, Rieger L, Kapp M, Sutterlin M, Dietl J, Kammerer U (2004) Indoleamine 2,3-dioxygenase (IDO) expression in invasive extravillous trophoblast supports role of the enzyme for materno-fetal tolerance. *J Reprod Immunol* 61: 79–86

Hung MC, Link W (2011) Protein localization in disease and therapy. *J Cell Sci* 124: 3381–3392

Jackson SP, Schoenwaelder SM, Goncalves I, Nesbitt WS, Yap CL, Wright CE, Kenche V, Anderson KE, Dopheide SM, Yuan Y *et al* (2005) PI 3-kinase p110beta: a new target for antithrombotic therapy. *Nat Med* 11: 507–514

Jamieson S, Flanagan JU, Kolekar S, Buchanan C, Kendall JD, Lee WJ, Rewcastle GW, Denny WA, Singh R, Dickson J *et al* (2011) A drug targeting only p110alpha can block phosphoinositide 3-kinase signalling and tumour growth in certain cell types. *Biochem J* 438: 53–62

Juss JK, Hayhoe RP, Owen CE, Bruce I, Walmsley SR, Cowburn AS, Kulkarni S, Boyle KB, Stephens L, Hawkins PT *et al* (2012) Functional redundancy of class I phosphoinositide 3-kinase (PI3K) isoforms in signaling growth factor-mediated human neutrophil survival. *PLoS One* 7: e45933

Kieckbusch J, Balmas E, Hawkes DA, Colucci F (2015) Disrupted PI3K p110delta signaling dysregulates maternal immune cells and increases fetal mortality in mice. *Cell Rep* 13: 2817–2828

Koyasu S (2003) The role of PI3K in immune cells. *Nat Immunol* 4: 313–319

Kozakov D, Brenke R, Comeau SR, Vajda S (2006) PIPER: an FFT-based protein docking program with pairwise potentials. *Proteins* 65: 392–406

Kozakov D, Hall DR, Xia B, Porter KA, Padhorny D, Yueh C, Beglov D, Vajda S (2017) The ClusPro web server for protein-protein docking. *Nat Protoc* 12: 255–278

Lannutti BJ, Meadows SA, Herman SE, Kashishian A, Steiner B, Johnson AJ, Byrd JC, Tyner JW, Loriaux MM, Deininger M *et al* (2011) CAL-101, a p110delta selective phosphatidylinositol-3-kinase inhibitor for the treatment of B-cell malignancies, inhibits PI3K signaling and cellular viability. *Blood* 117: 591–594

Lee KM, Chuang E, Griffin M, Khattri R, Hong DK, Zhang W, Straus D, Samelson LE, Thompson CB, Bluestone JA (1998) Molecular basis of T cell inactivation by CTLA-4. *Science* 282: 2263–2266

Littlejohn TK, Takikawa O, Truscott RJ, Walker MJ (2003) Asp274 and his346 are essential for heme binding and catalytic function of human indoleamine 2,3-dioxygenase. *The Journal of biological chemistry* 278: 29525–29531

Mellor AL, Sivakumar J, Chandler P, Smith K, Molina H, Mao D, Munn DH (2001) Prevention of T cell-driven complement activation and inflammation by tryptophan catabolism during pregnancy. *Nat Immunol* 2: 64–68

Mondanelli G, Bianchi R, Pallotta MT, Orabona C, Albini E, Iacono A, Belladonna ML, Vacca C, Fallarino F, Macchiarulo A *et al* (2017a) A relay pathway between arginine and tryptophan metabolism confers immunosuppressive properties on dendritic cells. *Immunity* 46: 233–244

Mondanelli G, Iacono A, Allegrucci M, Puccetti P, Grohmann U (2019a) Immunoregulatory Interplay Between Arginine and Tryptophan Metabolism in Health and Disease. *Front Immunol* 10: 1565

Mondanelli G, Iacono A, Carvalho A, Orabona C, Volpi C, Pallotta MT, Matino D, Esposito S, Grohmann U (2019b) Amino acid metabolism as drug target in autoimmune diseases. *Autoimmun Rev* 18: 334–348

Mondanelli G, Ugel S, Grohmann U, Bronte V (2017b) The immune regulation in cancer by the amino acid metabolizing enzymes ARG and IDO. *Curr Opin Pharmacol* 35: 30–39

Munn DH, Zhou M, Attwood JT, Bondarev I, Conway SJ, Marshall B, Brown C, Mellor AL (1998) Prevention of allogeneic fetal rejection by tryptophan catabolism. *Science* 281: 1191–1193

Murphy JE, Padilla BE, Hasdemir B, Cottrell GS, Bunnett NW (2009) Endosomes: a legitimate platform for the signaling train. *Proc Natl Acad Sci USA* 106: 17615–17622

Nelp MT, Kates PA, Hunt JT, Newitt JA, Balog A, Maley D, Zhu X, Abell L, Allentoff A, Borzilleri R *et al* (2018) Immune-modulating enzyme

indoleamine 2,3-dioxygenase is effectively inhibited by targeting its apo-form. *Proc Natl Acad Sci USA* 115: 3249−3254

Okkenhaug K, Vanhaesebroeck B (2003) PI3K in lymphocyte development, differentiation and activation. *Nat Rev Immunol* 3: 317−330

Orabona C, Mondanelli G, Puccetti P, Grohmann U (2018) Immune checkpoint molecules, personalized immunotherapy, and autoimmune diabetes. *Trends Mol Med* 24: 931−941

Orabona C, Pallotta MT, Volpi C, Fallarino F, Vacca C, Bianchi R, Belladonna ML, Fioretti MC, Grohmann U, Puccetti P (2008) SOCS3 drives proteasomal degradation of indoleamine 2,3-dioxygenase (IDO) and antagonizes IDO-dependent tolerogenesis. *Proc Natl Acad Sci USA* 105: 20828−20833

Pallotta MT, Orabona C, Bianchi R, Vacca C, Fallarino F, Belladonna ML, Volpi C, Mondanelli G, Gargaro M, Allegrucci M *et al* (2014) Forced IDO1 expression in dendritic cells restores immunoregulatory signalling in autoimmune diabetes. *J Cell Mol Med* 18: 2082−2091

Pallotta MT, Orabona C, Volpi C, Vacca C, Belladonna ML, Bianchi R, Servillo G, Brunacci C, Calvitti M, Bicciato S *et al* (2011) Indoleamine 2,3-dioxygenase is a signaling protein in long-term tolerance by dendritic cells. *Nat Immunol* 12: 870−878

Prendergast GC, Mondal A, Dey S, Laury-Kleintop LD, Muller AJ (2018) Inflammatory reprogramming with IDO1 inhibitors: turning immunologically unresponsive 'Cold' tumors 'Hot'. *Trends Cancer* 4: 38−58

Puccetti P, Bianchi R, Fioretti MC, Ayroldi E, Uyttenhove C, Van Pel A, Boon T, Grohmann U (1994) Use of a skin test assay to determine tumor-specific CD8^{+} T cell reactivity. *Eur J Immunol* 24: 1446−1452

Puccetti P, Grohmann U (2007) IDO and regulatory T cells: a role for reverse signalling and non-canonical NF-kappaB activation. *Nat Rev Immunol* 7: 817−823

Romani L, Fallarino F, De Luca A, Montagnoli C, D'Angelo C, Zelante T, Vacca C, Bistoni F, Fioretti MC, Grohmann U *et al* (2008) Defective tryptophan catabolism underlies inflammation in mouse chronic granulomatous disease. *Nature* 451: 211−215

Stark AK, Sriskantharajah S, Hessel EM, Okkenhaug K (2015) PI3K inhibitors in inflammation, autoimmunity and cancer. *Curr Opin Pharmacol* 23: 82−91

Theate I, van Baren N, Pilotte L, Moulin P, Larrieu P, Renauld JC, Herve C, Gutierrez-Roelens I, Marbaix E, Sempoux C *et al* (2015) Extensive profiling of the expression of the indoleamine 2,3-dioxygenase 1 protein in normal and tumoral human tissues. *Cancer Immunol Res* 3: 161−172

Thomas SR, Salahifar H, Mashima R, Hunt NH, Richardson DR, Stocker R (2001) Antioxidants inhibit indoleamine 2,3-dioxygenase in IFN-gamma-activated human macrophages: posttranslational regulation by pyrrolidine dithiocarbamate. *J Immunol* 166: 6332−6340

Thorpe LM, Yuzugullu H, Zhao JJ (2015) PI3K in cancer: divergent roles of isoforms, modes of activation and therapeutic targeting. *Nat Rev Cancer* 15: 7−24

Vanhaesebroeck B, Guillermet-Guibert J, Graupera M, Bilanges B (2010) The emerging mechanisms of isoform-specific PI3K signalling. *Nat Rev Mol Cell Biol* 11: 329−341

Volpi C, Fallarino F, Pallotta MT, Bianchi R, Vacca C, Belladonna ML, Orabona C, De Luca A, Boon L, Romani L *et al* (2013) High doses of CpG oligodeoxynucleotides stimulate a tolerogenic TLR9-TRIF pathway. *Nat Commun* 4: 1852

Volpi C, Mondanelli G, Pallotta MT, Vacca C, Iacono A, Gargaro M, Albini E, Bianchi R, Belladonna ML, Celanire S *et al* (2016) Allosteric modulation of metabotropic glutamate receptor 4 activates IDO1-dependent, immunoregulatory signaling in dendritic cells. *Neuropharmacology* 102: 59−71